Journal of Inflammation Research

Dovepress
Taylor & Francis Group

Open Access Full Text Article

ORIGINAL RESEARCH

Inhibition of Hippocampal Neuronal Ferroptosis by Liproxstatin-1 Improves Learning and Memory Function in Aged Mice with Perioperative Neurocognitive Dysfunction

Liurong Lin[1,2,*], Xin Ling[1,2,*], Ting Chen[1,2,*], Qian Zhou[1,2], Jinghao Huang[1,2], Linshen Huang[1,2], Xianzhong Lin[1,2], Lanying Lin[1,2]

[1]Department of Anesthesiology, Anesthesiology Research Institute, The First Affiliated Hospital, Fujian Medical University, Fuzhou, Fujian, 350005, People's Republic of China; [2]Department of Anesthesiology, National Regional Medical Center, Binhai Campus of The First Affiliated Hospital, Fujian Medical University, Fuzhou, 350212, People's Republic of China

*These authors contributed equally to this work

Correspondence: Xianzhong Lin; Lanying Lin, Department of Anesthesiology, Anesthesiology Research Institute, The First Affiliated Hospital, Fujian Medical University, 20 Chazhong Road, Fuzhou, Fujian, 350005, People's Republic of China, Email linlanying@163.com

Background: Perioperative neurocognitive disorders (PND) are common in elderly patients after surgery, leading to long-term cognitive decline and reduced quality of life. The mechanisms are unclear, but ferroptosis, a key cell death pathway, may be involved in the disruption of brain homeostasis during perioperative stress.

Methods: In this study, we used the SAM-P8 mouse model to simulate brain aging and observe isoflurane-induced ferroptosis. Forty 8-month-old SAM-P8 mice were divided into four groups: control (CON), perioperative cognitive dysfunction (PND), PND with Liproxstatin-1 intervention (PND+Lip-1), and Liproxstatin-1 control (Lip-1). After 3% isoflurane anesthesia in the PND group, the PND+Lip-1 group received daily intrathecal Liproxstatin-1 injections for five days. Behavioral tests assessed spatial learning and memory. Nissl staining, transmission electron microscopy (TEM), FJB (Fluoro-Jade B), Western Blot (WB), and enzyme-linked immunosorbent assay (ELISA) evaluated neuronal morphology and levels of iron metabolism and lipid peroxidation markers.

Results: Behavioral tests indicated a decline in learning and memory function in the PND mice. Liproxstatin-1 treatment improved cognitive performance, restored normal neuron ratios, and alleviated mitochondrial damage. In the PND group, increased Cluster of Differentiation 71 (CD71) and decreased Ferroportin 1 (FPN1) and Glutathione Peroxidase 4 (GPx4) indicated ferroptosis activation, while Liproxstatin-1 normalized these markers, reduced ferrous ion concentration, Malondialdehyde (MDA), Reactive Oxygen Species (ROS), and 4-Hydroxy-2-nonenal (4-HNE) levels, and decreased Interleukin-6 (IL-6), showing anti-inflammatory effects.

Conclusion: The results of this study suggest that isoflurane-induced ferroptosis may play an important role in the pathologic progression of PND. The application of liproxstatin-1, a lipid peroxidation inhibitor, provides a new potential therapeutic target for perioperative neuroprotection.

Keywords: perioperative neurocognitive disorder, isoflurane, ferroptosis, lipid peroxidation, neuroprotection, SAM-P8 mice

Introduction

Aging is an irreversible and complex process[1] and is a major risk factor for neurodegenerative diseases.[2] As the number of aging population continues to rise, the incidence of diseases related to aging-induced decline in normal physiological functions of the body also continues to increase.[3] Perioperative neurocognitive disorders (PND) refers to neurocognitive changes associated with anesthesia and surgery, and is one of the most common neurological complications in the perioperative period, manifested by impaired learning and memory, deficits in attention and executive function.[4] PND may cause long-term cognitive decline, and perioperative stress exposures in conjunction with the accumulation of aging-

Received: 9 November 2024
Accepted: 13 February 2025
Published: 27 February 2025

associated molecular patterns in the central nervous system during the aging process are involved in disrupting the brain's internal environmental homeostasis.[5] This causes neural anatomical changes, alterations in the redox environment and low-grade chronic inflammation lead to neurodegenerative lesions, which in turn trigger pathological manifestations of neuronal and synaptic dysfunction related to cognitive function. However, little is known about the underlying pathogenic mechanisms of PND and effective treatments.

Over the past decades, studies of aging-related cognitive impairment have focused on the classical pathological features of neurodegenerative diseases such as Alzheimer's diseasein particular, deposition of amyloid plaques and aberrant phosphorylation of tau proteins.[6–8] These mechanisms have been suggested to be key contributors to the gradual decline of cognitive function; however, these studies have neglected the fact that aging occurs with systemic changes that occur during aging, particularly neuroinflammation associated with low-level chronic inflammatory responses and the potential blow from perioperative stress such as surgery or anesthesia.[9] Recent studies have shown that aging is not only accompanied by metabolic dysregulation within the neurons but also is closely associated with a chronic, low-level inflammatory response within the central nervous system (CNS), and that this Inflammatory responses further weaken the brain's ability to cope with external stresses.[10] In the perioperative period, acute stresses induced by surgery and anesthesia are superimposed on this state of vulnerability, potentially exacerbating cognitive impairment in elderly patients, yet mechanistic studies in this area remain limited.

Ferroptosis has received attention as a nonapoptotic cell death mechanism, especially in the study of end-stage pathology in neurodegenerative diseases such as Alzheimer's disease and Parkinson's disease.[11] However, the role of ferroptosis during the unique window of the perioperative period has not been explored. Ferroptosis, a form of cell death triggered by iron accumulation and lipid peroxidation, differs from other types of cell death in that it is dependent on dysregulation of iron metabolism and overproduction of reactive oxygen species (ROS). Although its role in advanced neurodegenerative diseases has been revealed, whether it is involved in the development of PND has not been clearly established. In previous studies, ferroptosis inhibition strategies have usually employed classical ferroptosis inhibitors such as deferoxamine and ferrostatin-1.[12,13] These drugs are mostly administered by intraperitoneal injection, caudal vein injection, or cerebral stereotactic injection in animal experiments.[14] However, these modes of administration usually require larger doses of the drug, which may cause greater experimental animal. However, these modes of administration usually require larger drug doses and may cause greater damage to experimental animals, especially the direct intervention of stereotactic injection on the central nervous system may bring a certain degree of trauma or stress reaction. We used intrathecal injection as the route of administration, which is a more efficient way of drug delivery that not only achieves precise drug delivery but also significantly reduces trauma and stress to the experimental animals.[15] We also chose liproxstatin-1, a direct inhibitor of lipid peroxidation, to be used in this study. This inhibitor is able to block lipid peroxidation, a key component of ferroptosis, more effectively[16] and thus clarify the specific role of lipid peroxidation in neuronal ferroptosis.

In terms of animal models, previous studies have used natural aging animals or classical Alzheimer's disease animal models to simulate the phenotype of cognitive impairment; however, in this experiment, the SAM-P8 mouse model was used, which is an ideal model for studying cognitive decline and neurological damage associated with aging. The SAM-P8 mice showed obvious signs of natural aging after 6 months of age[17,18], and in comparison to the naturally aging The mice retain strong locomotor ability and experimental tolerance, allowing them to provide stable data during invasive manipulations and behavioral tests, and reducing mortality during experiments. Compared to the classic Alzheimer's disease mouse model, the SAM-P8 mice not only mimic the pathological changes in the aging brain but also represent the overall aging state of the aging brain in a more comprehensive manner. The association of dysregulated iron metabolism during surgery and after anesthesia with PND is becoming increasingly evident, and an in-depth exploration of the ferroptosis mechanism will provide new insights into understanding of the pathological mechanisms of perioperative cognitive dysfunction.

The aim of this study was to verify that perioperative isoflurane promotes ferroptosis causing cognitive impairment by exacerbating lipid peroxidation in aging neurons, and that Liproxstatin-1 can effectively ameliorate this pathological process. In this study, SAM-P8 mice were exposed to isoflurane anesthesia to simulate perioperative stress conditions, and the occurrence of ferroptosis in hippocampal neurons was examined. Behavioral tests,

such as Morris Water Maze (MWM), were used to assess the spatial learning and memory abilities of the mice. We also used Western Blot (WB) and Enzyme-Linked Immunosorbent Assay (ELISA) to detect neuroinflammatory indicators, oxidative/antioxidant-related molecules, and cognitive impairment-related molecules, such as tau hyperphosphorylation. These analyses aimed to assess whether isoflurane induces PND through ferroptosis at the molecular and pathological levels and to explore the neuroprotective effect of liproxstatin-1 on hippocampal neurons. This study will not only reveal the potential pathological mechanisms of ferroptosis in perioperative cognitive impairment, but also provide new therapeutic targets for perioperative cognitive protection in elderly patients.

Materials and Methods

Animal Grouping and Intervention

All animal experiments in this study were reviewed and approved by the Animal Ethics Committee of Fujian Medical University (Approval Number: IACUC FJMU 2024–0196). The mice used in the experiments were obtained from Beijing Huafukang Biotechnology Co., Ltd. (Production License No.: SCKX (Jing) 2024–0003) and had a baseline body weight of approximately 30–33g. They were housed in an SPF-grade animal facility under controlled conditions, with an ambient temperature of 22 ± 1°C and a humidity level of 50%. All experimental procedures adhered to EU Directive 2010/63/EU for the protection and welfare of animals used in scientific research.

Forty male mice were divided into 4 groups according to the random number table method: CON group (n = 10), PND group (n = 10), PND+Lip-1 group (n=10), and Lip-1 group (n = 10). The PND group and PND+Lip-1 group were exposed to 3% isoflurane (RWD Life Science Co., Ltd., Shenzhen, China) for 5 hours using a small animal anesthesia machine (RWD Life Science Co., Ltd., Shenzhen, China), and the remaining two groups were exposed for the same length of time.[19] The remaining two groups were exposed to an air-oxygen gas mixture for the same duration. Seven days after the end of the exposure, the PND+Lip-1 and Lip-1 groups received intrathecal injections of 4 mg/kg of Liproxstatin-1 solution (Selleck Chemicals, Houston, Texas, China) formulated with 2% DMSO, 40% PEG300, 2% Tween80, and 56% ddH2O, and the rest of the groups received the same duration of exposure 56% ddH_2O, while the remaining two groups were injected with the same volume of saline using the same intrathecal injection method. The following procedure was used for intrathecal injection in mice: Mice were anesthetized with an intraperitoneal injection of pentobarbital sodium (40 mg/kg) and placed in a prone position with the tail gently extended to expose and highlight the L5-L6 intervertebral space. The skin over the injection site was disinfected with alcohol swabs to ensure asepsis. A fine needle was then inserted into the L5-L6 intervertebral space at a 15–30° angle, directed cranially. The needle was advanced slowly until a loss of resistance was felt, indicating entry into the subarachnoid space. The solution was injected slowly and steadily, after which the needle was gently withdrawn. Slight pressure was applied to the injection site using an alcohol swab to prevent bleeding or leakage. The mouse was placed on a pre-warmed heating pad and observed until full recovery, ensuring the absence of adverse reactions before returning it to its housing. Three days after the injection, we performed the open field experiment, the new object recognition experiment, and the water maze experiment, and after all the behavioral experiments were completed, we took the materials to complete the subsequent molecular experiments.

Behavioral Tests

Open Field Test (OFT)

The OFT system (Shanghai Jiliang Software Technology Co. Ltd, Shanghai, China) was used to detect spontaneous activity behavior and exploratory behavior in mice. The OFT was used to evaluate spontaneous activity and exploratory behavior in mice. Each mouse was placed in the center of an 80 cm × 80 cm × 40 cm acrylic box and allowed to explore freely for 5 minutes. A digital camera mounted above the box recorded their activity, and video tracking software was used to analyze the total distance traveled, time spent in the center zone, and the number of center crossings. Between tests, the apparatus was cleaned with 75% ethanol to remove odors.

New Object Recognition Experiment (NOR)

The experiment was conducted using the new object recognition system (Shanghai Jiliang Software Technology Co. Ltd, Shanghai, China) in three phases for three days. In the first stage, the mice were placed in the device without any objects and were free to move around for 5 min. In the second stage, the mice were familiarized with the new object recognition system by placing two identical cubes symmetrically at the opposite corners of the device to make sure that the cubes did not have any smells and were fixed so that they could not be moved. A camera device and software were used to record the exploration time of the mice on each object, and the number of times the animals explored each object and the time were measured within 5 min. In the third stage, one of the two cubes was replaced by a cylinder, and the mice were also placed into the device to explore for 5 min. The recognition time of the old and new objects was recorded by the software, and the recognition time of the new object was recorded as Tn, and the recognition time of the old object was recorded as Tf. The Recognition Index (RI) was calculated as: RI=Tn/(Tn+Tf). The setup of the surroundings was kept constant throughout the experimental test. To eliminate odor effects, the experimental setup was cleaned with 75% ethanol after each mouse test.

Morris Water Maze (MWM)

(1) Positioning Navigation Experiment

Conducted in a closed circular pool (diameter 100 cm, height 50 cm), the animals' behavior during the test was automatically recorded with a digital video camera located above the task device, and the video tracking software automatically analyzed the animal's action trajectory (Shanghai Xinsoft Information Co, LTD, Shanghai, China). A transparent circular escape platform (12 cm in diameter) was fixed in the center of the third quadrant, submerged 2 cm below the surface of the water. The water temperature was consistently maintained at 26°C throughout the experimental period to ensure standardized conditions. Pure water was used in the maze, and no additional dyes were added. Mice were randomly placed into the water facing the wall of the pool from a fixed position in all four quadrants, in a different order each day. Each mouse had 60s to find the hidden platform, and the time between entering the water and finding the hidden platform was called the escape latency. If the mice could not reach the platform within 60s, they were guided to find the platform and stayed on it for 15s to learn. Every day, each mouse repeated the above steps in 4 quadrants for 4 days.

(2) Space Exploration Experiment

The day after the localization navigation experiment, the platform was removed, and the mice were put into the pool from the quadrant opposite to the original platform for 60s, and the video recording analysis software was used to record the number of times the mice crossed the designated platform area within 60s, in order to evaluate the spatial memory cognitive ability of the mice.

Mouse Sample Collection

Anesthesia

Mice were anesthetized with an intraperitoneal injection of 0.3% sodium pentobarbital at 45 mg/kg. Anesthesia was confirmed by the absence of eyelash and corneal reflexes, reduced muscle tone, and lack of response to skin pinching. The mouse was then placed in a supine position on a dissection table.

Cardiac Exposure

The abdominal fur was shaved, and the area was disinfected with iodine. A midline incision was made from the pubic area to the xiphoid process to expose the abdominal cavity. The diaphragm was cut along both sides, and the sternum was opened along the midline to expose the heart.

Perfusion

The pericardium was carefully opened, and the apex of the heart was gently stabilized with forceps. A 20-gauge catheter was inserted into the left ventricle toward the aorta. After observing blood return, the stylet was removed, and the catheter was secured. The right atrium was immediately incised to allow blood to drain. Perfusion was initiated with

normal saline at a flow rate of approximately 50 mL/min, starting fast and then slowing down. Once the blood turned clear and the liver turned pale, perfusion was switched to 4% paraformaldehyde.

Brain Tissue Collection and Fixation

When the fixative reached the brain, muscle twitching in the limbs was observed. After the mouse stopped twitching and the tissues became rigid, the cervical spine was severed using a guillotine, and the skin was removed. The skull was carefully opened with bone scissors to expose the brain, which was then completely removed and placed in 4% paraformaldehyde for 24 hours. The brain was subsequently processed for paraffin embedding.

Pathology Testing

Nissl Staining

Dewax the paraffin sections by immersing them in xylene I and II (20 min each), followed by absolute ethanol I and II (5 min each), and 75% ethanol (5 min). Rinse with tap water, stain with Nissl solution (1:100 dilution, Biosharp, China) for 2 minutes, then wash and briefly differentiate with 1% glacial acetic acid. After rinsing, dry in an oven. Clear sections in xylene for 5 minutes and mount with neutral resin.

Transmission Electron Microscopy (TEM)

Fresh 1 mm^3 tissue samples were trimmed to the size of a wheat grain and immediately placed in tubes containing 2.5% glutaraldehyde for fixation at 4°C for 12–24 hours. Samples were rinsed three times with 0.1M PBS (pH 7.2), then fixed in 1% osmium tetroxide for 2 hours, followed by PBS rinses and water washes. Dehydration was performed in a graded ethanol series (30% to 100%) and 100% acetone. Samples were infiltrated with 812 embedding medium (SPI, 90529–77-4) at increasing concentrations and polymerized at 70°C for 24 hours. Ultra-thin sections (70–100 nm) were cut, mounted on copper grids, stained with uranyl acetate and lead citrate, and observed under a transmission electron microscope at 80 kV.

Fluoro-Jade B (FJB) Staining

Paraffin sections were deparaffinized and hydrated, followed by incubation with 50% acetic acid for 10 minutes. Sections were then stained with 0.0004% Fluoro-Jade B solution (Beijing Solarbio Science&Technology Co., Ltd, Beijing, China) and counterstained with DAPI. Stained sections were examined under a fluorescence microscope with the following excitation/emission wavelengths: DAPI (330–380 nm/420 nm), FJB (465–495 nm/515–555 nm).

Immunofluorescence

After fixation with 4% PFA for 30 min at room temperature, each section was rinsed twice (5 min each) with PBS. The sections were then treated with 3% bovine serum albumin for 30 min at room temperature to block nonspecific binding sites. Sections were incubated overnight at 4°C with the primary antibody to the target protein, NeuN (1:300 dilution, Abcam Plc, Cambridge, UK). The following day, sections were rinsed with PBS and then incubated with secondary antibody at room temperature for 1 h. DAPI staining was performed. Stained sections were visualized using a fluorescence microscope and images were acquired.

Molecular Detection

WB

Fresh hippocampal tissue (30 mg) was homogenized in 300 μL RIPA lysis buffer with phosphatase and protease inhibitors. After homogenization and 30 minutes of lysis on ice, samples were centrifuged at 12,000 rpm for 10 minutes at 4°C. The supernatant was collected as the total protein solution. Following protein quantification and denaturation, samples were subjected to SDS-PAGE and transferred to PVDF membranes. Membranes were blocked for 20 minutes, incubated overnight at 4°C with primary antibodies (Abcam Plc, Cambridge, UK), and then incubated with secondary antibodies (Thermo Fisher Scientific, Waltham, Massachusetts, USA) for 1 hour at room temperature. Protein bands were visualized with ECL and analyzed using ImageJ, with gray values normalized to internal controls.

ELISA

ELISA kits for IL-10, IL-6, ROS, MDA, and GSH (ABclonal Biotechnology Co., Ltd., Wuhan, China) were used according to manufacturer instructions. Samples and standards were added to plates, incubated with enzyme-labeled reagents, washed, and developed with color reagents. Absorbance was measured at 450 nm, and concentrations were calculated based on a standard curve, adjusted for dilution factors.

Ferrous Ion Content

The Ferrous Iron Colorimetric Assay Kit (Elabscience Biotechnology Co., Ltd., Wuhan, China) was used to measure iron content. Tissue homogenates were prepared, centrifuged, and supernatants were added to the assay plates with color reagent, incubated, and measured at 593 nm.

Statistical Analysis

Data were analyzed using GraphPad Prism 9.0. Normally distributed data were expressed as mean ± SD and analyzed by one-way ANOVA with the least significant difference (LSD) test used for post hoc comparisons. Non-normally distributed data were analyzed using the Kruskal–Wallis *H*-test. For time-course data, repeated measures ANOVA was performed. Sample sizes were determined using the Resource Equation Approach, considering the exploratory nature of the study and challenges in estimating standard deviation and effect size. Each group included 10 animals, accounting for statistical robustness and potential experimental losses. A p-value <0.05 was considered statistically significant.

Results

Behavioral Tests

OFT

(1) Activity Trajectory: During the experimental period, the activity levels of mice in all groups were normal (Figure 1B), with no significant difference in total distance traveled. Representative movement trajectories were selected for comparison. As shown in Figure 1A, compared to the CON group, mice in the PND group tended to move around the periphery of the apparatus, with reduced time and distance in the central area. The PND+Lip-1 group showed improvement relative to the PND group, while the Lip-1 group had similar movement patterns to the CON group.

(2) Central Area Activity Time: Kruskal–Wallis *H*-test showed a significant difference in central area activity time among groups ($z = 10.566$, $P = 0.014$) (Figure 1C). Pairwise comparisons revealed: (1) a statistically significant difference between the PND and CON groups ($z = 2.821$, $P = 0.005$), with PND mice spending less time in the central area; (2) the PND group also spent less time in the central area compared to the Lip-1 group ($z = 2.658$, $P = 0.008$).

NOR

(1) Activity Trajectory: Representative trajectories from each group showed that PND mice spent less time exploring the novel object and exhibited reduced movement within the activity area compared to the other groups (Figure 2A).

(2) Recognition Index: During the NOR test, all groups displayed normal activity levels (Figure 2B). Analysis of the recognition index for the novel object revealed statistically significant differences among groups ($F = 33.888$, $P < 0.001$). LSD post hoc comparisons (Figure 2C) indicated: (1) a significant difference between the CON and PND groups $P < 0.001$), with the CON group showing more interest in the novel object; (2) significant differences between the PND group and both the PND+Lip-1 and Lip-1 groups $P < 0.001$), with the PND group showing less exploration of the novel object; (3) no significant difference between the PND+Lip-1 and CON groups ($P = 0.084$); (4) no significant difference between the Lip-1 and CON groups ($P = 0.266$).

MWM

(1) Swimming Speed: Analysis of swimming speeds in the Morris Water Maze showed no statistically significant differences among groups ($F = 2.236$, $P = 0.086$) (Figure 3B).

(2) Movement Trajectory Changes: Representative trajectories from the MWM test (Figure 3A) showed that on Day 1 of the navigation test, PND and Lip-1 mice exhibited more wall-hugging behavior and longer, more disorganized paths

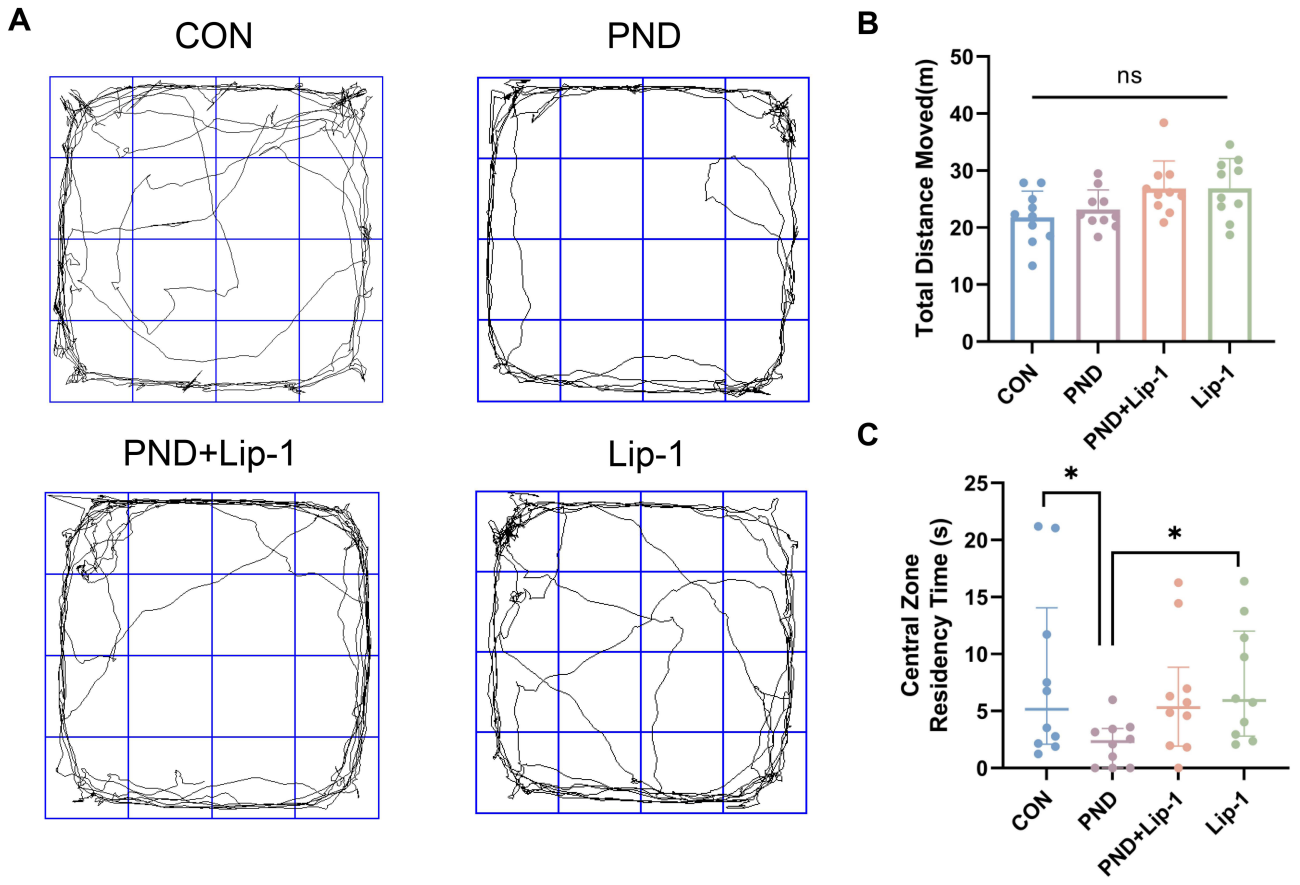

Figure 1 OFT analysis of cognitive function in mice.
Notes: (**A**) Open field test results show the movement trajectories of each group (CON, PND, PND+Lip-1, Lip-1).(**B**) Total distance moved in the open field test shows no significant differences across groups. (**C**) Central zone residency time indicates a significant reduction in the PND group compared to the CON and PND+Lip-1 groups, suggesting anxiety-like behavior in the PND group. Data are presented as mean ± SEM (n=10/group). Compared with PND group *P < 0.05.
Abbreviation: ns, statistically non-significant.

compared to the CON group. By Day 4, the CON group quickly located the platform, while the PND+Lip-1 and Lip-1 groups showed improvement with shorter paths compared to the PND group.

(3) Escape Latency: Repeated measures ANOVA showed significant differences in escape latency over 4 days among groups ($F = 941.127$, $P < 0.001$), with significant group-time interaction ($F = 7.973$, $P < 0.001$) (Figure 3C). Post-hoc Bonferroni analysis on Day 4 indicated: (1) a significant difference between the CON and PND groups ($P = 0.001$), with longer escape latency in the PND group; (2) a significant reduction in escape latency in the PND+Lip-1 group compared to the PND group $P < 0.001$); (3) the PND+Lip-1 group had a longer latency than the CON group ($P = 0.001$); (4) the Lip-1 group had a longer latency than the CON group ($P = 0.033$).

(4) Spatial Exploration: In the spatial probe test, platform crossings in the third quadrant were analyzed (Figure 3D). ANOVA showed a significant difference among groups ($F = 2.962$, $P = 0.045$). LSD pairwise comparisons indicated a significant difference between the PND and Lip-1 groups ($P = 0.0268$), with fewer platform crossings in the PND group.

Pathology Results

Nissl Staining

As shown in Figure 4A, Nissl staining of the CON group reveals typical hippocampal architecture, characterized by neurons arranged in a regular and dense pattern, clear staining, and uniform distribution of Nissl bodies. The Lip-1 group

https://doi.org/10.2147/JIR.S503784

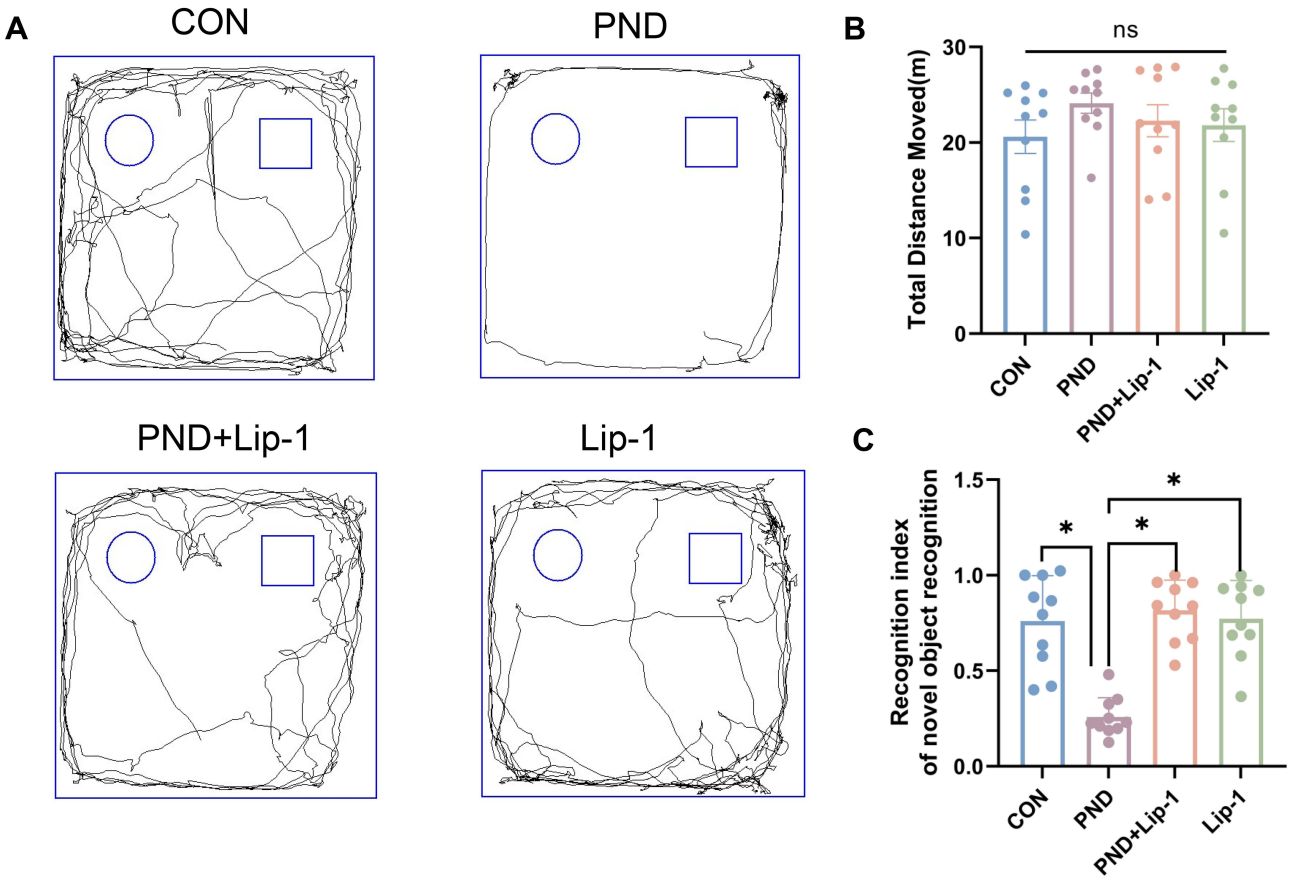

Figure 2 NOR for memory assessment.
Notes: (**A**) Representative movement trajectories in the novel object recognition test for all groups. (**B**) Total distance moved indicates no significant differences between groups. (**C**) The recognition index of novel object recognition shows a significant decrease in the PND group compared to the CON group, while Lip-1 treatment (PND+Lip-1) restores recognition ability. Data are presented as mean ± SEM (n=10/group). Compared with PND group *P < 0.05.
Abbreviation: ns, statistically non-significant.

exhibits similar features to the CON group across all regions. In contrast, the PND group shows a sparse neuronal arrangement in the hippocampal area, with significantly expanded intercellular spaces, prominent nuclear condensation, and uneven distribution of Nissl bodies. The hippocampal structure in the PND+Lip-1 group is similar to the CON group, with neurons arranged in a relatively orderly manner, although scattered nuclear condensation is still observed. Kruskal–Wallis test results indicate significant differences among groups (P = 0.016). Figure 4B demonstrates a statistically significant difference in the apoptosis rate between the CON and PND groups (P = 0.013), with a significantly higher rate of abnormal neurons in the PND group. Although the difference between the PND+Lip-1 and PND groups is not statistically significant, there is a reduction in the abnormal neuron rate in the PND+Lip-1 group, suggesting a protective effect of Liproxstatin-1 in the PND model.

TEM

Figure 4C illustrates that in the CON group, neurons in the hippocampal CA1 region display intact mitochondrial structures, clear nuclear membranes, and normal cristae without noticeable organelle damage or pathological changes. Compared to the CON group, the PND group shows typical ferroptosis features, including swollen mitochondria, loss of cristae, rupture of the outer membrane, and irregular morphological changes in the nuclear membrane. These alterations indicate severe mitochondrial dysfunction in PND neurons, consistent with the ultrastructural characteristics of ferroptosis. In the PND+Lip-1 group, after treatment with the ferroptosis inhibitor Liproxstatin-1, the pathological features of ferroptosis are alleviated, with relatively intact mitochondrial morphology, partial preservation of cristae, and clearer

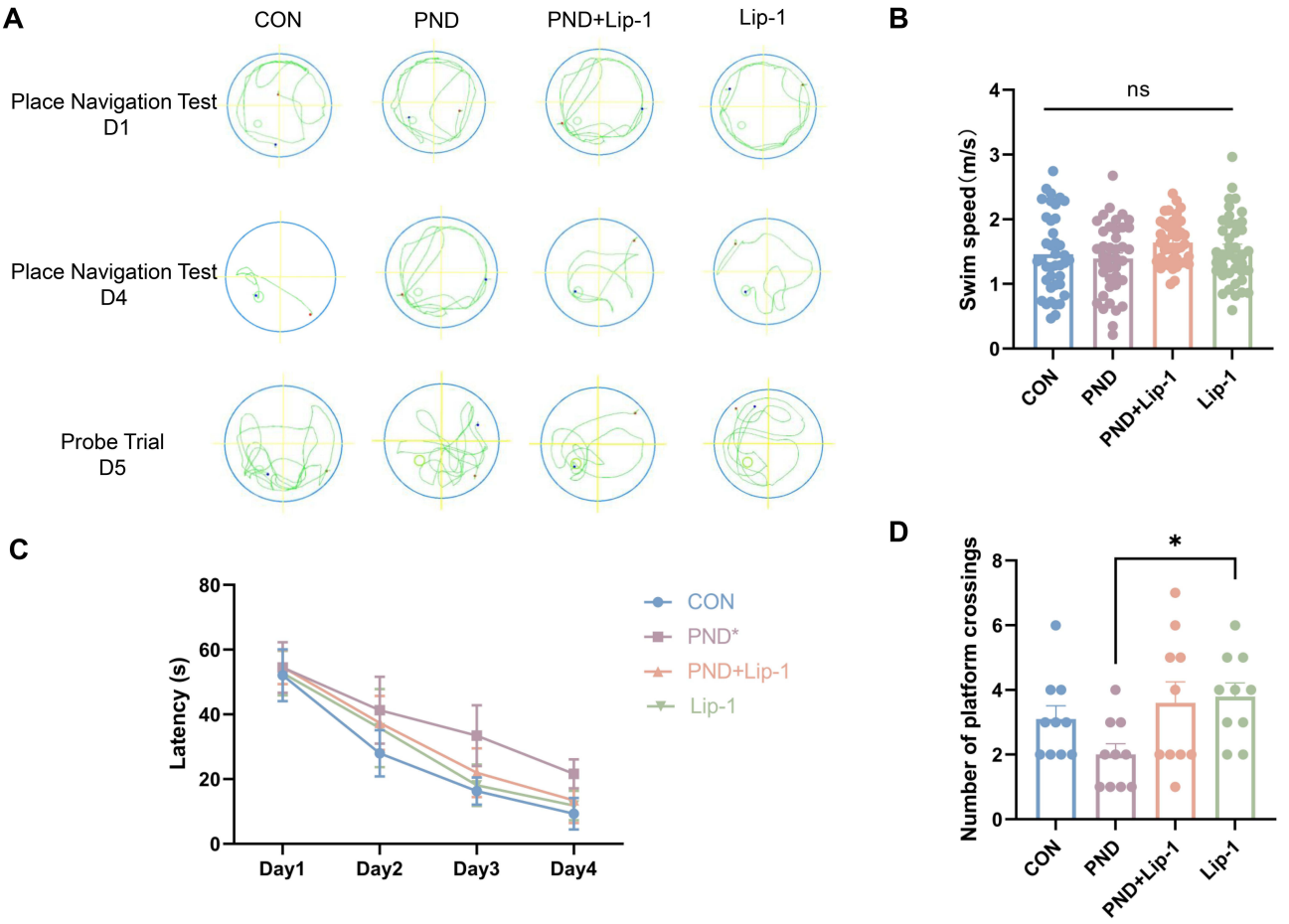

Figure 3 MWM evaluating spatial learning and memory.
Notes: (**A**) Representative swim paths from the place navigation test on day 1 (D1) and day 4 (D4), and the probe trial on day 5 (D5) for all groups. (**B**) Swim speed shows no significant differences between groups. (**C**) Latency to find the platform over four training days shows no significant differences. (**D**) The number of platform crossings in the probe trial on day 5 shows a significant reduction in the PND group, which is improved by Lip-1 treatment. Data are presented as mean ± SEM (n=10/group). Compared with PND group *P < 0.05.
Abbreviation: ns, statistically non-significant.

nuclear membrane structure, indicating a protective effect of Liproxstatin-1 on mitochondria. The Lip-1 group, when compared to the CON group, does not display ferroptosis ultrastructural characteristics; mitochondrial morphology and nuclear membrane integrity are consistent with the CON group, further validating the efficacy of Lip-1 in preventing ferroptosis.

Immunofluorescence and Western Blot Results

Figure 5A showed the results of immunofluorescence staining of NeuN, a neuronal marker. The PND group showed significantly weaker fluorescence intensity of NeuN compared to the CON group (P = 0.0224). The quantitative fluorescence results in Figure 5C showed stronger fluorescence intensity of NeuN in the PND+Lip-1 group compared to the PND group (P = 0.0128), suggesting that Liproxstatin-1 had a protective effect on neurons. Figure 5B showed the results of FJB staining, which was specifically used to label neuronal degeneration. Figure 5D showed a significant increase in the fluorescence intensity of FJB in the PND group (P=0.0036), indicating increased neuronal degeneration in this group; in contrast, the intensity of FJB staining in the PND+Lip-1 group was significantly weaker (P = 0.0009).

Figure 5E WB results showing p-Tau and total Tau expression in hippocampal homogenates. Compared with the CON group, the expression of p-Tau was increased in the PND group. Figure 5F Further quantitative analysis of the

https://doi.org/10.2147/JIR.S503784

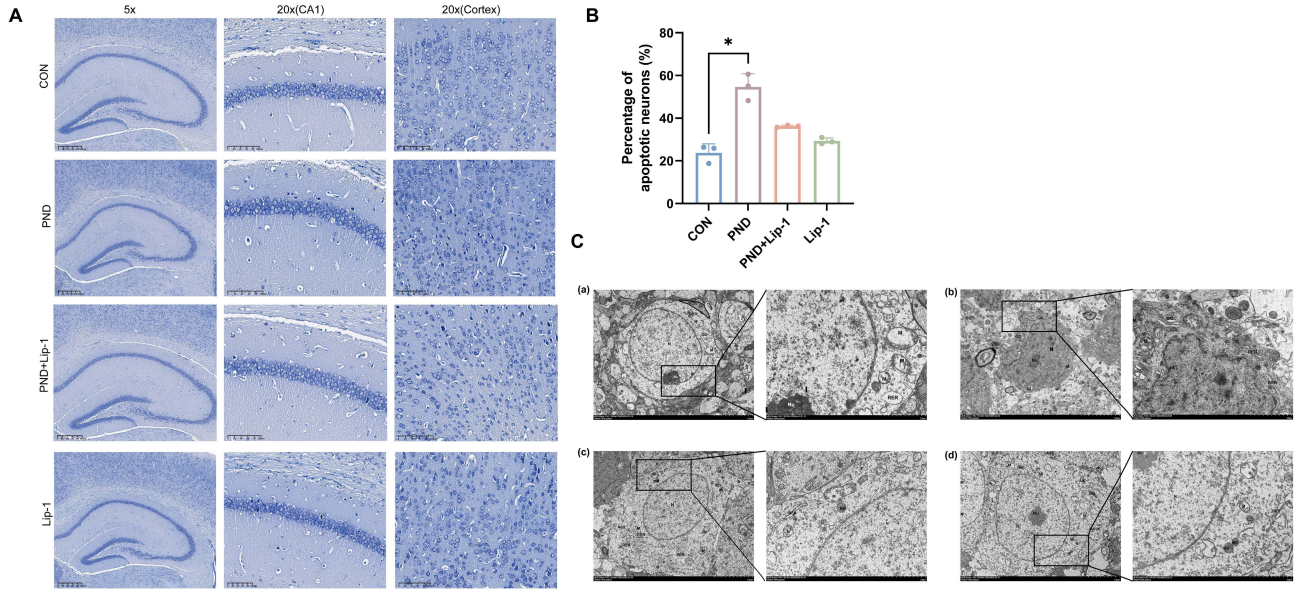

Figure 4 Histological and ultrastructural analysis of hippocampal neurons.
Notes: (**A**) Nissl staining of the hippocampal CA1 region shows a reduction in neuronal density in the PND group compared to the CON and PND+Lip-1 groups. (**B**) Quantification of Nissl-stained neurons in the CA1 region, with the PND group showing significantly fewer neurons than the CON group. (**C**) TEM images of hippocampal neurons. The PND group shows mitochondrial swelling and disrupted membranes, typical of ferroptosis, while the PND+Lip-1 group exhibits reduced mitochondrial damage. Data are presented as mean ± SEM (n=3/group). Compared with PND group *P < 0.05.

p-Tau/Tau ratio showed that the p-Tau/Tau ratio in the PND group was significantly higher than that in the CON group (P = 0.0079), suggesting that the aberrant phosphorylation of Tau protein was increased in the PND group, which was closely related to the development of cognitive dysfunction.

Expression of Ferroptosis-Related Proteins

Figure 6A shows the expression levels of GPx4 and CD71 by Western blot analysis. The results indicate a significant decrease in GPx4 expression and a significant increase in CD71 expression in the PND group compared to the CON group, suggesting ferroptosis-related pathological changes in the PND model. In the PND+Lip-1 group, treated with the ferroptosis inhibitor Liproxstatin-1, GPx4 expression was significantly restored, and CD71 expression decreased. The Lip-1 group showed expression patterns similar to the CON group, with no signs of ferroptosis. Figures 6B and C provide quantitative analyses of GPx4 and CD71 protein expression, further confirming that GPx4 expression was significantly lower in the PND group compared to the CON group (P < 0.0001), while CD71 expression was significantly higher (P = 0.0001). In the PND+Lip-1 group, GPx4 expression significantly increased (P < 0.0001), and CD71 expression significantly decreased (P = 0.0052), showing no significant difference from the CON group.

Figure 6D displays the expression levels of 4-HNE, BDNF, and FPN1. In the PND group, 4-HNE expression was significantly elevated, indicating increased oxidative stress, while BDNF and FPN1 expressions were significantly reduced, suggesting neuronal damage and iron homeostasis disruption. In the PND+Lip-1 group, 4-HNE expression decreased, and BDNF and FPN1 expressions partially recovered, indicating a neuroprotective effect of Liproxstatin-1 in the PND model.

Figures 6E, F and J provide quantitative analyses of 4-HNE, FPN1, and BDNF protein expression, respectively. The results show that 4-HNE expression in the PND group was significantly higher than in the CON group (P < 0.0001), while FPN1 and BDNF expressions were significantly lower (P < 0.0001). In the PND+Lip-1 group, 4-HNE expression was reduced (P < 0.0001), and both FPN1 (P = 0.0207) and BDNF expressions significantly recovered (P < 0.0001).

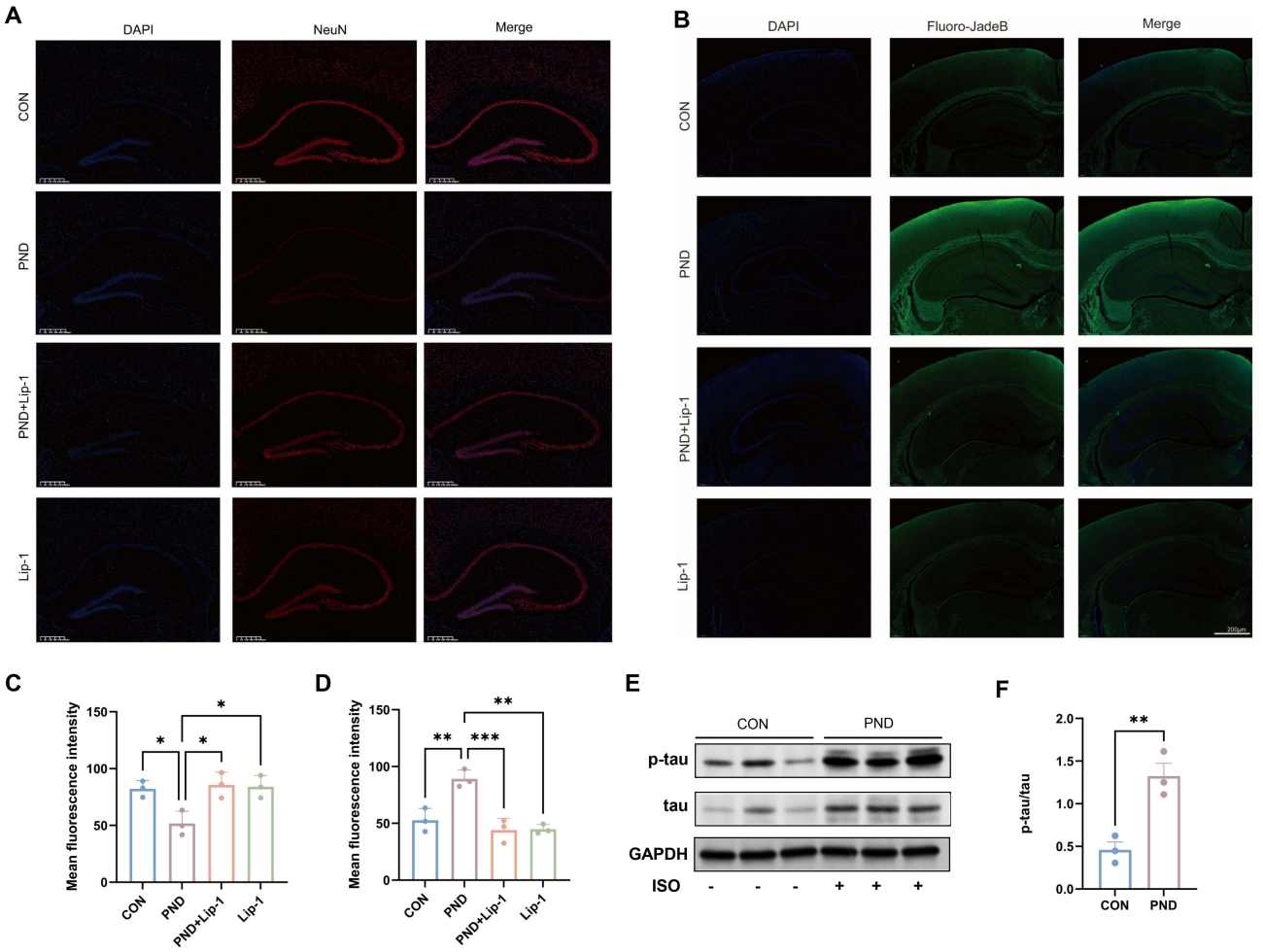

Figure 5 NeuN and Fluoro-Jade B staining to assess neuronal survival and degeneration in the hippocampus.
Notes: (**A**) Immunofluorescence staining of NeuN shows decreased neuronal survival in the PND group, while PND+Lip-1 treatment preserves neuronal integrity. (**B**) Fluoro-Jade B staining highlights increased neuronal degeneration in the PND group, which is reduced in the PND+Lip-1 group. (**C** and **D**) Quantification of mean fluorescence intensity for NeuN and Fluoro-Jade B. Significant differences are observed between CON and PND groups, with partial recovery in the PND+Lip-1 group. (**E** and **F**) Western blot analysis and quantification of p-Tau and total Tau expression in hippocampal homogenates. The PND group shows an increased p-Tau/Tau ratio compared to the CON group, while Liproxstatin-1 treatment reduces p-Tau levels, indicating a neuroprotective effect. Data are presented as mean ± SEM (n=3/group). Compared with PND group *P < 0.05, **P < 0.01, ***P < 0.001.

Oxidative Stress, Ferrous Ion Content and Inflammatory Indicators

Figure 7 illustrates the differences in oxidative stress markers, ferrous ion content, and inflammatory indicators across different groups. Figure 7A MDA concentration reflected the degree of lipid peroxidation. The MDA concentration in the PND group was significantly higher than that in the CON group ($P < 0.0001$), suggesting a significant increase in the level of oxidative stress. In the PND+Lip-1 group, the MDA concentration was significantly lower ($P < 0.0001$), approaching the level of the CON group, suggesting that Lip-1 was effective in alleviating oxidative stress. Figure 7B GSH concentration indicated antioxidant capacity. The GSH concentration in the PND group was significantly lower than that in the CON group ($P = 0.002$), indicating a decreased antioxidant defense ability. In contrast, GSH concentration in the PND+Lip-1 group rebounded significantly ($P = 0.0483$), indicating that Lip-1 had a restorative effect on the antioxidant capacity. Figure 7C ROS level is an important marker of oxidative stress. The ROS level in the PND group was significantly higher than that in the CON group ($P = 0.011$), while that in the PND+Lip-1 group was significantly lower ($P = 0.0003$), close to the CON group, further suggesting that Lip-1 can effectively reduce oxidative stress. Figure 7D Ferrous ion concentration reflected changes in iron homeostasis. The ferrous ion concentration in the PND group was significantly higher than that in the CON group ($P = 0.0003$), indicating an imbalance in iron homeostasis, which may be associated with ferroptosis. The

https://doi.org/10.2147/JIR.S503784

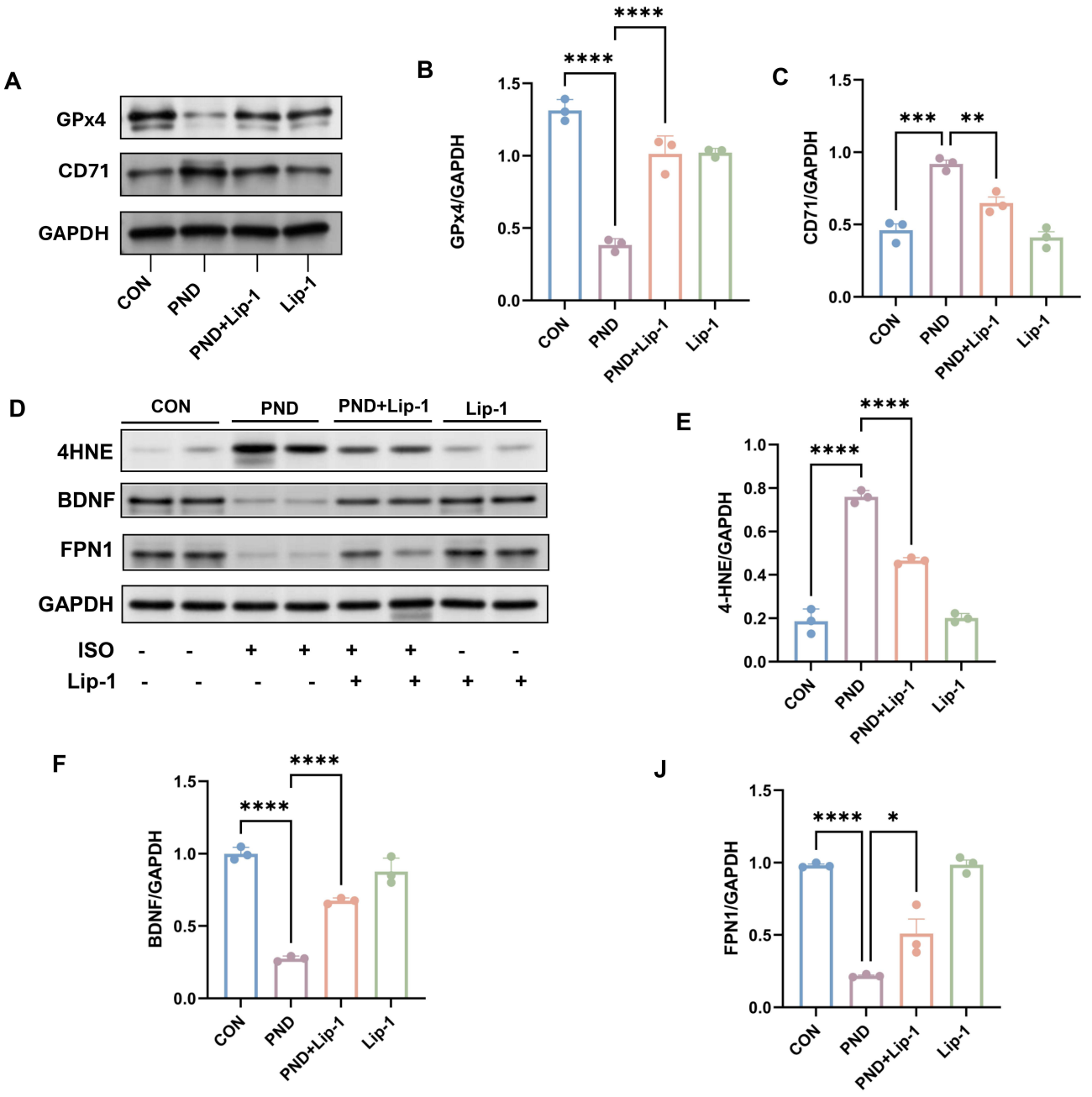

Figure 6 Lipid peroxidation, iron regulation, and neuroprotection markers in mice.

Notes: (**A**) Western blot analysis of GPx4 and CD71 protein expression. (**B**) GPx4 expression is significantly reduced in the PND group, restored in the PND+Lip-1 group. (**C**) CD71 expression is increased in the PND group and reduced after Liproxstatin-1 treatment. (**D**) Western blot analysis of 4-HNE, BDNF, and FPN1 proteins shows oxidative stress markers and neurotrophic factors. (**E**) Quantification of 4-HNE, showing increased levels in PND, which are reduced by Liproxstatin-1. (**F** and **J**) FPN1 and BDNF levels indicate neuroprotection in the PND+Lip-1 group. Data are presented as mean ± SEM (n=3/group). Compared with PND group * P < 0.05, **P < 0.01, ****P < 0.001, ****P < 0.0001.

ferrous ion concentration in the PND+Lip-1 group was significantly lower (P = 0.0106), indicating that Liproxstatin-1 was able to restore iron homeostasis. Figure 7E and F) IL-10 and IL-6 are anti-inflammatory and pro-inflammatory cytokines, respectively. The concentration of IL-10 was significantly decreased in the PND group (P < 0.0001), and the concentration of IL-6 was significantly increased in the PND group (P = 0.0006), suggesting that there was an inflammatory response in the PND group. There was a certain degree of increase in IL-10 concentration and a significant decrease in IL-6 concentration in the PND+Lip-1 group (P = 0.0002), suggesting that Liproxstatin-1 has a modulating effect on inflammation.

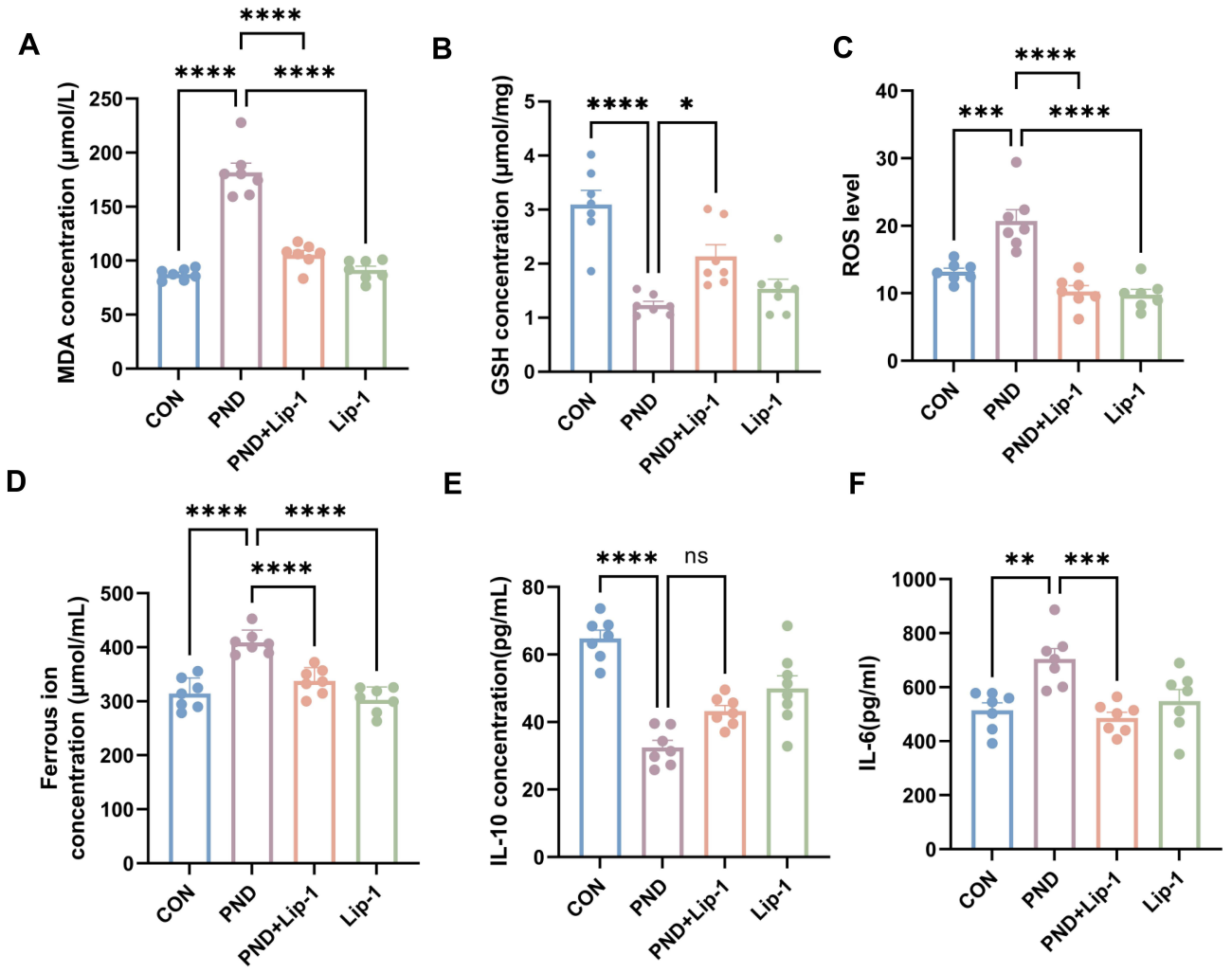

Figure 7 Oxidative stress markers and cytokine levels in mice.
Notes: (**A**) MDA concentrations are significantly elevated in the PND group and reduced with Liproxstatin-1 treatment. (**B**) GSH concentrations are decreased in the PND group, partially restored in the PND+Lip-1 group. (**C**) ROS levels are elevated in the PND group, and Liproxstatin-1 reduces oxidative stress. (**D**) Ferrous ion concentrations are elevated in the PND group, indicating ferroptosis, and are reduced with Liproxstatin-1 treatment. (**E** and **F**) IL-10 and IL-6 concentrations show significant inflammatory changes in the PND group, with Liproxstatin-1 restoring anti-inflammatory balance. Data are presented as mean ± SEM (n=7/group). Compared with PND group *P < 0.05, **P < 0.01, ***P < 0.001, ****P < 0.001.

Discussion

We found that SAM-P8 mice exposed to isoflurane in a PND model showed cognitive impairment, impaired learning and memory and an increased proportion of abnormal neurons. Hippocampal neurons in PND mice underwent an imbalance of iron homeostasis as well as ferroptosis, which exacerbated the neurodegenerative process. Neuronal ferroptosis was accompanied by a disruption of the oxidative/antioxidant system balance, and the use of Liproxstatin-1 effectively attenuated lipid peroxidation in neurons. In addition, Liproxstatin-1 partially restored the balance of iron metabolism and mitochondrial damage. These results suggest that ferroptosis may be one of the causes of neurodegeneration in PND and that inhibition of this process with Liproxstatin-1 is a potential therapeutic strategy to alleviate the cognitive decline associated with PND.

First, intrathecal injection of Liproxstatin-1 was effective in exerting neuroprotective effects. In behavioral tests at the functional level, PND mice that received Liproxstatin-1 intervention showed better spatial learning memory ability in MWM. Pathologic results showed that the percentage of cells with normal neurons in the cortex of PND mice showed a decrease in Nysted staining compared to controls, and the percentage of normal neurons increased after receiving Liproxstatin-1 intervention. In addition Brain-Derived Neurotrophic Factor (BDNF) in the hippocampus of PND mice

https://doi.org/10.2147/JIR.S503784

after the administration of Liproxstatin-1, one of the markers of neuronal repair, appeared to be elevated to a certain extent compared to PND mice Also demonstrated previous studies on the neuroprotective effect of Liproxstatin-1, which is similar to our findings. Therefore, the present study extends the application of ferroptosis inhibitors for therapeutic modification of perioperative neurocognitive deficits, and although Liproxstatin-1 had been shown to attenuate ferroptosis in models of stroke and traumatic brain injury,[20] this was the first study that demonstrated its efficacy in preventing neurodegeneration in a model of PND. Liproxstatin-1 was able to ameliorate cognition in PND mice deficits, reduced mitochondrial damage, and restore iron homeostasis in PND mice, which offered new insight for therapeutic interventions targeting ferroptosis in the perioperative period.

Second, Liproxstatin-1 exerted its role by inhibiting ferroptosis in hippocampal neurons to a certain extent, suggesting that ferroptosis was involved in the process of PND-induced neurodegenerative changes in hippocampal nerves. In recent years, the key pathogenic role of ferroptosis in neurodegenerative diseases had received increasing attention. Because iron ions were involved in many biological processes in the central nervous system, such as oxygen transport, myelin phospholipid production, and neurotransmitter synthesis and metabolism,[21] an imbalance in iron metabolism had been suggested as one of the initiating factors of neuronal degeneration. In the PND mouse model of the present study, the brain had elevated levels of ferrous ions and increased expression of the molecule CD71, a molecule related to cellular iron metabolism, and decreased FPN1. CD71 is the major iron uptake receptor, and transports iron into the cell by binding to transferrin.[22] FPN1 was regulated by hepcidin, which can bind to FPN1 and causes its degradation, reducing iron export.[23] In the present study, PND mice showed accumulation of ferrous ions in neurons after simulated perioperative stress exposure, increased expression of CD71 on cell membranes further caused intracellular accumulation of ferric ions, and elevated levels of iron-over-regulated ferredoxin induced by an imbalance in iron metabolism inhibited the activity of FPN1, which in turn limited the release of ferric ions from the intracellular iron pool. These results are consistent with previous molecular pathological alterations of ferroptosis in different disease models and cell types. And our study demonstrated for the first time that ferroptosis played an equally important role in PND pathology, where elevated intracellular concentrations of iron ions in neuronal cells exacerbated oxidative damage in susceptible neuronal cells due to senescence, facilitating the continued progression of multiple pathological manifestations and ultimately leading to severe cognitive impairment.

An imbalance in the oxidative/antioxidant system in hippocampal neurons of PND mice triggers ferroptosis in hippocampal neurons leading to the development of cognitive impairment. Due to the accumulation of lipid peroxidation metabolites 4-HNE, ROS, and MDA in neurons caused by isoflurane exposure, the key antioxidant molecules GPx4 and GSH were depleted, which further led to elevated oxidative stress burden causing ferroptosis, and the accumulation of peroxides led to the impairment of membrane integrity, which caused the dysfunction of intracellular free iron transport in and out of the cell, further aggravating the ferroptosis in the hippocampus. Dysfunction led to dysregulation of intracellular transport of free iron in and out of the cell, further exacerbating ferroptosis.[24] In addition, accumulation of lipid peroxides triggered a free radical cascade, further generating more ROS and increasing intracellular oxidative stress levels. In this study, the application of the inhibitor Liproxstatin-1 promoted the increase of hippocampal GPx4 and GSH levels and decreased ROS production in PND mice, thereby inhibiting the expression of molecules related to the ferroptosis process, suggesting that the key supply pathway for the regulation of intracellular ferroptosis in neurons in PND was the reduction of glutathione/glutathione peroxidase 4 (Glutathione- Glutathione peroxidase 4 (GSH/GPx4) pathway.

The GSH/GPx4 system was repaired in PND mice receiving Liproxstatin-1, suggesting that it played an important role in the maintenance of cellular redox homeostasis. GSH was the most abundant non-protein thiol in neurons that exerted antioxidant defense and maintains redox homeostasis,[25,26] and GPx4 was an important antioxidant enzyme that inhibited lipid peroxidation. The results of this study confirmed the above findings and linked the modulation of this critical pathway to the pathological manifestations of cognitive impairment, in which reduced levels of GSH in the CNS were associated with neuronal degeneration and may be involved in the progression of pathologic alterations in the nervous system. GSH maintained redox homeostasis by binding to intracellular free iron and served as a substrate for the lipid detoxification mediated by GPx4.[26] When GPx4 activity was inhibited or expression was reduced, cellular sensitivity to ferroptosis was increased. The impaired metabolism of intracellular lipid oxides, which in turn were

abnormally metabolized by iron ions,[27] generated large amounts of lipids that disrupt intracellular redox homeostasis and attacked biomolecules, triggering cell death. In some cases, ferroptosis was also accompanied by the process of cell necrosis.[28] When GSH was reduced in neurons, the reduced GPx4 then fails to function as an antilipid peroxidant. Following the catalytic process of the Fenton reaction, polyunsaturated fatty acid peroxides (PUFA-OOH) can accumulate to lethal levels to trigger ferroptosis.[29] PUFA-OOH were highly reactive oxides, and their accumulation in cellular membranes disrupted membrane integrity, leading to cellular structural instability. It also activated multiple kinases related to tau phosphorylation, and upon activation these kinases exerted excessive phosphorylation modifications on tau proteins, leading to dissociation of tau proteins from microtubules and the formation of insoluble aggregates, which further affected the normal structure and function of neurons. This may be the cause of tau hyperphosphorylation and neuronal damage.

In addition, lipid peroxidation exacerbates the inflammatory response in the CNS. In this study senescent mice receiving isoflurane exposure induced elevation of the inflammatory factor interleukin-6 (IL-6), in addition to the occurrence of neuronal ferroptosis accompanied by accumulation of ferric ions inhibited the intracellular anti-inflammatory response, leading to a decrease in the level of IL-10. Other models of neurodegenerative diseases confirmed that pathological changes associated with cognitive impairment triggered the release of other inflammatory factor signals from reactive microglia, leading to increased iron uptake and cell death in neurons.[30] Combined with previous findings and the results of the present experiments, it was hypothesized that low-grade inflammatory signals accumulated during aging as well as diminished levels of oxidative stress after exposure to perioperative stress cause an increase in GSH- GPx4 axis expression in neurons and neural support cells was diminished leading to accumulation of iron ions and oxidative metabolic substrates thereby triggering ferroptosis in hippocampal neurons leading to cellular dysfunction. Our study emphasized that ferroptosis was a key oxidative stress-related pathway that exacerbates neuronal damage in PND.

This study highlights the clinical significance of targeting ferroptosis in perioperative neurocognitive dysfunction (PND), a leading cause of postoperative cognitive decline in elderly patients. Despite the high incidence of PND, its underlying pathogenesis remains poorly understood. Our findings identified ferroptosis as a key mechanism driving PND and demonstrated the therapeutic potential of Liproxstatin-1 in mitigating cognitive impairment through its targeted inhibition of lipid peroxidation. By preserving mitochondrial integrity, reducing oxidative stress, and modulating signaling pathways such as Nrf2/HO-1, Liproxstatin-1 safeguards hippocampal neuronal viability and synaptic integrity, providing a mechanistic basis for its neuroprotective effects. Clinically, Liproxstatin-1 offers a focused approach to addressing the oxidative and ferroptotic damage exacerbated by anesthesia and surgery, particularly in vulnerable elderly patients. Compared to existing therapies, its targeted action against ferroptosis represents a novel and promising strategy for improving postoperative cognitive outcomes. Moreover, the potential applications of Liproxstatin-1 extend beyond PND, with implications for treating other neurodegenerative diseases characterized by ferroptosis and oxidative stress. Future research should focus on determining the optimal dosage and timing of Liproxstatin-1 administration, exploring its synergistic effects with other neuroprotective agents, and assessing its efficacy in broader contexts, such as age-related or surgery-induced cognitive disorders like Alzheimer's disease or delirium. Addressing these areas will further elucidate its therapeutic potential and support its translation into clinical practice. In summary, targeting ferroptosis with agents like Liproxstatin-1 could pave the way for groundbreaking advances in perioperative neuroprotection and the management of neurodegenerative conditions.

Limitations

Despite the encouraging results of this study, we must recognize some limitations. First, this study only compared the levels of oxidative stress and inflammatory factors between different groups, thus confirming the effect of Liproxstatin-1 in suppressing inflammatory responses and oxidative stress. However, inflammatory responses and oxidative stress may have dynamic changes in the pathological process of PND. Future studies could perform multiple assays at different time points to better understand the time-dependent effects of Liproxstatin-1 on inflammation and oxidative stress, thus validating the therapeutic effects at different stages. In addition, our study focused on the hippocampus, a brain region critical for memory, but other cognitively related brain regions, such as the prefrontal cortex, were only observed

pathologically and not studied in greater depth at the molecular level. In the future, it could be investigated whether ferroptosis also plays a role in the remaining brain regions. Second, only typical lipid peroxidation products (MDA and 4-HNE) were detected in the present study so as to assess the level of lipid peroxidation, but there may be differences in the role of different types of lipid peroxidation products in cellular damage. Follow-up studies could detect changes in multiple lipid peroxidation products by more precise methods such as mass spectrometry analysis and metabolomics to understand the role of different lipid peroxidation products in PND pathology.

Conclusion

This study highlights lipid peroxidation as a key trigger of ferroptosis in hippocampal neurons, contributing to the pathology of PND. We found that anesthesia and surgery significantly exacerbated iron metabolism imbalance and oxidative stress in the hippocampus, leading to neuronal apoptosis, abnormal tau protein phosphorylation, and cognitive dysfunction. Liproxstatin-1 demonstrated a strong neuroprotective effect by reducing lipid peroxidation, alleviating oxidative stress, and promoting neuronal survival. This intervention helped restore iron metabolism balance and improved cognitive outcomes, underscoring its potential as a therapeutic agent for PND. These findings emphasize the role of anesthesia and surgery in triggering cognitive impairments through oxidative stress and ferroptosis, while positioning Liproxstatin-1 as a promising strategy to mitigate these effects. Further research into the mechanisms linking surgical stress and neurodegeneration could pave the way for innovative treatments targeting lipid peroxidation in PND and related conditions.

Acknowledgments

This study was funded by the Fujian Province Young and Middle-aged Teacher Education Research Project (Project No. JAT220100).

Disclosure

The authors report no conflicts of interest in this work.

References

1. López-Otín C, Blasco MA, Partridge L, Serrano M, Kroemer G. Hallmarks of aging: an expanding universe. *Cell*. 2023;186(2):243–278. doi:10.1016/j.cell.2022.11.001
2. Pan Y, Nicolazzo JA. Impact of aging, Alzheimer's disease and Parkinson's disease on the blood-brain barrier transport of therapeutics. *Adv Drug Deliv Rev*. 2018;135:62–74. doi:10.1016/j.addr.2018.04.009
3. Lloyd-Sherlock P, McKee M, Ebrahim S, et al. Population ageing and health. *Lancet*. 2012;379(9823):1295–1296. doi:10.1016/S0140-6736(12)60519-4
4. Evered LA, Silbert BS. Postoperative Cognitive Dysfunction and Noncardiac Surgery. *Anesth Analg*. 2018;127(2):496–505. doi:10.1213/ANE.0000000000003514
5. Ransohoff RM. How neuroinflammation contributes to neurodegeneration. *Science*. 2016;353(6301):777–783. doi:10.1126/science.aag2590
6. Long JM, Holtzman DM. Alzheimer disease: an update on pathobiology and treatment strategies. *Cell*. 2019;179(2):312–339. doi:10.1016/j.cell.2019.09.001
7. Selkoe DJ, Hardy J. The amyloid hypothesis of Alzheimer's disease at 25 years. *EMBO Mol Med*. 2016;8(6):595–608. doi:10.15252/emmm.201606210
8. Busche MA, Hyman BT. Synergy between amyloid-β and tau in Alzheimer's disease. *Nat Neurosci*. 2020;23(10):1183–1193. doi:10.1038/s41593-020-0687-6
9. Heneka MT, Kummer MP, Latz E. Innate immune activation in neurodegenerative disease. *Nat Rev Immunol*. 2014;14(7):463–477. doi:10.1038/nri3705
10. Franco R, Fernández-Suárez D. Alternatively activated microglia and macrophages in the central nervous system. *Prog Neurobiol*. 2015;131:65–86. doi:10.1016/j.pneurobio.2015.05.003
11. Bergsland N, Tavazzi E, Schweser F, et al. Targeting iron dyshomeostasis for treatment of neurodegenerative disorders. *CNS Drugs*. 2019;33(11):1073–1086. doi:10.1007/s40263-019-00668-6
12. Yang WS, SriRamaratnam R, Welsch ME, et al. Regulation of ferroptotic cancer cell death by GPX4. *Cell*. 2014;156(1–2):317–331. doi:10.1016/j.cell.2013.12.010
13. Miotto G, Rossetto M, Di Paolo ML, et al. Insight into the mechanism of ferroptosis inhibition by ferrostatin-1. *Redox Biol*. 2020;28:101328. doi:10.1016/j.redox.2019.101328
14. Ding XS, Gao L, Han Z, et al. Ferroptosis in Parkinson's disease: molecular mechanisms and therapeutic potential. *Ageing Res Rev*. 2023;91:102077. doi:10.1016/j.arr.2023.102077

15. Hambright WS, Fonseca RS, Chen L, Na R, Ran Q. Ablation of ferroptosis regulator glutathione peroxidase 4 in forebrain neurons promotes cognitive impairment and neurodegeneration. *Redox Biol*. 2017;12:8–17. doi:10.1016/j.redox.2017.01.021
16. Stockwell BR, Friedmann Angeli JP, Bayir H, et al. Ferroptosis: a regulated cell death nexus linking metabolism, redox biology, and disease. *Cell*. 2017;171(2):273–285. doi:10.1016/j.cell.2017.09.021
17. Reale M, Costantini E, Aielli L, et al. Proteomic signature and mRNA expression in hippocampus of SAMP8 and SAMR1 mice during aging. *Int J Mol Sci*. 2022;23(23):15097. doi:10.3390/ijms232315097
18. Griñán-Ferré C, Corpas R, Puigoriol-Illamola D, Palomera-ávalos V, Sanfeliu C, Pallàs M. Understanding epigenetics in the neurodegeneration of alzheimer's disease: SAMP8 mouse model. *J Alzheimers Dis*. 2018;62(3):943–963. doi:10.3233/JAD-170664
19. Zhou Q, Zheng Z, Chen C, et al. Activation of ACE2/Ang-(1–7)/Mas axis improves cognitive dysfunction induced by isoflurane in mice via inhibiting oxidative stress. *J Anesthesia Transl Med*. 2024;3(3):123–131. doi:10.1016/j.jatmed.2024.09.003
20. Wang D, Zhang S, Ge X, et al. Mesenchymal stromal cell treatment attenuates repetitive mild traumatic brain injury-induced persistent cognitive deficits via suppressing ferroptosis. *J Neuroinflammation*. 2022;19(1):185. doi:10.1186/s12974-022-02550-7
21. Ward RJ, Zucca FA, Duyn JH, Crichton RR, Zecca L. The role of iron in brain ageing and neurodegenerative disorders. *Lancet Neurol*. 2014;13(10):1045–1060. doi:10.1016/S1474-4422(14)70117-6
22. Gomme PT, McCann KB, Bertolini J. Transferrin: structure, function and potential therapeutic actions. *Drug Discov Today*. 2005;10(4):267–273. doi:10.1016/S1359-6446(04)03333-1
23. Vogt ACS, Arsiwala T, Mohsen M, Vogel M, Manolova V, Bachmann MF. On iron metabolism and its regulation. *Int J Mol Sci*. 2021;22(9):4591. doi:10.3390/ijms22094591
24. Hirschhorn T, Stockwell BR. The development of the concept of ferroptosis. *Free Radic Biol Med*. 2019;133:130–143. doi:10.1016/j.freeradbiomed.2018.09.043
25. Iskusnykh IY, Zakharova AA, Pathak D. Glutathione in brain disorders and aging. *Molecules*. 2022;27(1):324. doi:10.3390/molecules27010324
26. Hider RC, Kong XL. Glutathione: a key component of the cytoplasmic labile iron pool. *Biometals*. 2011;24(6):1179–1187. doi:10.1007/s10534-011-9476-8
27. Yang WS, Kim KJ, Gaschler MM, Patel M, Shchepinov MS, Stockwell BR. Peroxidation of polyunsaturated fatty acids by lipoxygenases drives ferroptosis. *Proc Natl Acad Sci U S A*. 2016;113(34):E4966–4975. doi:10.1073/pnas.1603244113
28. Gao W, Wang X, Zhou Y, Wang X, Yu Y. Autophagy, ferroptosis, pyroptosis, and necroptosis in tumor immunotherapy. *Signal Transduct Target Ther*. 2022;7(1):196. doi:10.1038/s41392-022-01046-3
29. Belaidi AA, Masaldan S, Southon A, et al. Apolipoprotein E potently inhibits ferroptosis by blocking ferritinophagy. *Mol Psychiatry*. 2022;28. doi:10.1038/s41380-022-01568-w
30. Sterling JK, Kam TI, Guttha S, et al. Interleukin-6 triggers toxic neuronal iron sequestration in response to pathological α-synuclein. *Cell Rep*. 2022;38(7):110358. doi:10.1016/j.celrep.2022.110358